ORIGINAL REPORT



Frictional weakening of a granular sheared layer due to viscous rolling revealed by discrete element modeling

Alexandre Sac-Morane^{1,2} • Manolis Veveakis¹ • Hadrien Rattez²

Received: 5 April 2023 / Accepted: 5 February 2024 / Published online: 3 March 2024 © The Author(s), under exclusive licence to Springer-Verlag GmbH Germany, part of Springer Nature 2024

Abstract

Considering a 3D sheared granular layer through a discrete element modeling, it is well known the rolling resistance influences the macro friction coefficient. Even if the rolling resistance role has been deeply investigated previously because it is commonly used to represent the shape and the roughness of the grains, the rolling viscous damping coefficient is still not studied. This parameter is rarely used or only to dissipate the energy and to converge numerically. This paper revisits the physical role of those coefficients with a parametric study of the rolling friction and the rolling damping at different shear speeds and different confinement pressures. It has been observed the damping coefficient induces a frictional weakening. Indeed, competition between the rolling resistance and the rolling damping occurs. Angular resistance aims to avoid grains rolling, decreasing the difference between the angular velocities of grains. Whereas, angular damping acts in the opposite, avoiding a change in the difference between the angular velocities of grains. In consequence, grains stay rolling and the sample toughness decreases. This effect must be considered to not overestimate the frictional response of a granular layer.

Keywords Discrete element method · Rolling parameter · Sheared layer friction · Granular materials

1 Introduction

Accurately measuring or calculating the frictional strength of granular sheared layers is of paramount importance across all fields of granular media-related sciences, including earth-quakes and fault mechanics [1, 2], landslides [3], and debris flows [4] to name but a few. It is very well accepted nowadays that the calculation of a macroscopic property like the frictional coefficient of granular media is the result of grainto-grain interactions at the micro-scale [5, 6]. Therefore, in

Manolis Veveakis and Hadrien Rattez have contributed equally to this work.

Alexandre Sac-Morane alexandre.sac-morane@uclouvain.be

Manolis Veveakis manolis.veveakis@duke.edu

Hadrien Rattez hadrien.rattez@uclouvain.be

- Multiphysics Geomechanics Lab, Duke University, Durham 27708, NC, USA
- Institute of Mechanics, Materials and Civil Engineering, UCLouvain, Louvain-la-Neuve 1348, Belgium

order to accurate capture those effects and homogenize them to the friction coefficient of a layer, higher order analytical and numerical approaches need to be considered [7–9].

One of the most well-accepted approaches in direct modeling of granular media is the Discrete Element Method [10]. Two main types of models exist for this approach: a non-regularized formulation [11] and a regularized one [12]. The first one, called the Contact Dynamics Method, considers particles do not overlap and their motion is controlled by shocks and friction. The second one has been designed to consider interactions between grains, computed with calibrated parameters and overlaps. The latter description is used here as the applications targeted in the present paper involve large stresses for which the deformation of the grains cannot be ignored.

The discrete element method started with a simple linear contact law [14, 15], but since then contact laws have been modified [16]: (i) considering grain crushing [17, 18], (ii) introducing the effect of pressure solution [19–21], (iii) exploring the effect of contact healing [22, 23], (iv) appreciating the influence of the cohesion in between the grains due to cementation [24–26] or (v) the cohesion induced by capillary bridges [27] among others. Also, it allows some to focus on the temperature influence, identifying the pressurization of



the pore fluid [28, 29] and grain melting [30, 31] as the main phenomena driving the evolution of the frictional strength of a fault zone during large crustal events.

The present work is motivated by previous numerical studies modelling fault zones [10, 23, 32] that used various contact laws to capture and understand the experimental behavior observed on sheared fault zone materials, and the main goal is to assess the influence on global behavior of contact laws and parameters values. Even though different relevant outputs for dense granular flows are reviewed by the French research group *Groupement de Recherche Milieux Divisés* (GDR MiDi) [33], we are focused in this paper on the macro friction coefficient at steady state. Notice that the influence on this parameter, among others, of the local friction, the particle shape and the rolling resistance has already been investigated with the Contact Dynamic formulation [34, 35]. However, in the present study, we focus on the influence of the rolling contact laws between grains on the macroscopic strength of a granular sheared layer with a regularized description. Indeed, experimental results [36, 37], and numerical ones [38-40] have highlighted that grain rolling has a significant impact on the mechanical behavior with many rolling models being formulated since [41, 42]. In the literature the elastic-plastic spring dashpot model is identified as the benchmark for this response [43, 44] and has been extended to conclude that: (i) rolling helps the formation of shear bands and decreases the sample strength [45–48]; (ii) the stress-dilatancy curves are modified [49–51] when accounting for the rolling resistance coming from intragranular friction [52, 53] and roughness [54–56].

The computational cost of discrete element simulations is not negligible, and especially if grains clusters [57], superquadric particles [58] or polyhedral shapes [59–61] are assumed to approximate the shape, those simulations become quickly computationally costly. Because of that, laws relating the grain shape and the rolling friction have been developed [62–64]. This has enabled simulations to keep using round particles with a rolling resistance stemming from an equivalent shape, allowing to take into account the particles shape at a lower computational cost. However, the introduced angular damping influence is not well constrained, hence being neglected in most of the DEM simulations or only used for stability reasons [42, 43] rather than for physical robustness [65]. In this work we revisit the physical role of the rolling resistance in a granular sheared layer and perform a parametric study over the rolling friction and the rolling viscous damping coefficients to understand better their influence on the macroscopic friction coefficient of a granular sheared layer.

2 Theory and formulation

The Discrete Element Model (DEM) is an approach developed by Cundall & Strack [12] to simulate granular materials at the particles level. The foundation of this method is to consider inside the material the individual particles and their interactions explicitly. Newton's laws (linear and angular momentum) are used to compute the motion of the grains, formulated as follows for one grain:

$$m\frac{\partial v_i}{\partial t} = mg_i + f_i \tag{1}$$

$$I\frac{\partial \omega_i}{\partial t} = M_i \tag{2}$$

where m is the particle mass, v_i the particle velocity vector, g_i the gravity acceleration vector, f_i the sum of contact force vectors applied to the particle, I the moment of inertia of the particle, ω_i the angular velocity vector, M_i the sum of contact moment vectors applied to the particle (torques due to rolling and to the tangential forces).

Considering two particles with radii R^1 and R^2 , the interaction between particles is computed only if the distance between grains satisfies the following inequality:

$$\overline{x_i^1 - x_i^2} < R^1 + R^2 \tag{3}$$

where x_i^1 (resp. x_i^2) is the center of the particle 1 (resp. 2) and $\overline{u_i}$ is the norm of the vector u_i . Once contact is detected between grains 1 and 2, the normal vector of the contact n_i^{12} is computed as $n_i^{12} = (x_i^1 - x_i^2)/x_i^1 - x_i^2$. Then the normal overlap vector Δ_{ni} and the tangential overlap vector Δ_{ti} are determined.

$$\Delta_{ni} = \left(R^1 + R^2 - \left(x_j^1 - x_j^2\right)n_j^{12}\right)n_i^{12} \tag{4}$$

The tangential component Δ_{ii} is computed incrementally, integrating the relative tangential velocity between particles during the contact.

$$\Delta_{ti} = \Delta_{ti} + v_{ti}^{12} \times dt \tag{5}$$

where v_{ti}^{12} is the relative tangential velocity vector defined at the relation 6 and dt is the time step used in the simulation.

$$v_{ii}^{12} = v_i^{12} - \left(v_i^{12} n_i^{12}\right) n_i^{12} \tag{6}$$



$$\begin{split} v_i^{12} &= v_i^1 - v_i^2 + (R^1 - \delta/2)\epsilon_{ijk}n_j^{12}\omega_k^1 \\ &+ (R^2 - \delta/2)\epsilon_{ijk}n_i^{12}\omega_k^2 \end{split} \tag{7}$$

where v_i^{12} is the relative velocity vector between grains and $\delta = \Delta_{ni} n_i^{12}$ is the norm of the normal overlap vector. Notice that the terms $(R - \delta/2)$ represent the corrected radii at the contact. Here, the angular velocities ω_i of the grains are considered to compute the tangential overlap vector Δ_{ii} . As the contact orientation can evolve with time, it is important to update by rotation and scaling the tangential overlap vector $\Delta_{ii}^{new} = \Delta_{ii}^{old} - \Delta_{ii}^{old} n_i^{12} n_i^{12}$ and $\overline{\Delta_{ii}^{new}} = \Delta_{ii}^{old}$.

A relative angular velocity vector $\Delta \omega_i$ is also needed to compute the rolling behavior.

$$\Delta\omega_i = \omega_i^1 - \omega_i^2 \tag{8}$$

The contact models between cohesionless particles obey the Hertz contact theory [66]. Normal, tangential and angular models are shown at Fig. 1 and described in the following.

As contact can happen between particles with different properties, some equivalent parameters need to be defined. The equivalent radius R^* and equivalent mass m^* are defined at equations 9 and 10 with an harmonic mean.

$$\frac{1}{R^*} = \frac{1}{R^1} + \frac{1}{R^2} \tag{9}$$

$$\frac{1}{m^*} = \frac{1}{m^1} + \frac{1}{m^2} \tag{10}$$

The equivalent Young modulus Y^* and shear modulus G^* are defined at equations 11 and 12 with an harmonic mean adjusted by Poisson's ratio.

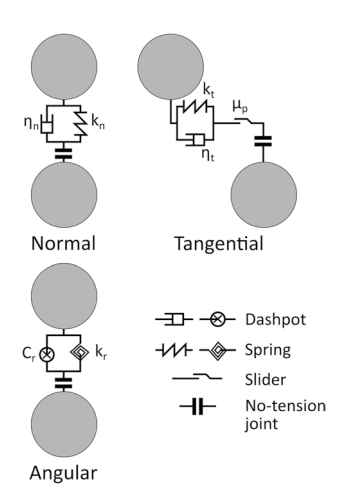


Fig. 1 The contact between two particles obeys to normal, tangential and rolling elastic-plastic spring-dashpot laws

$$\frac{1}{Y^*} = \frac{1 - v^{1^2}}{Y^1} + \frac{1 - v^{2^2}}{Y^2}$$

$$\iff Y^* = \frac{Y}{2(1 - v^2)}$$
(11)

$$\frac{1}{G^*} = \frac{2(2 - v^1)(1 + v^1)}{Y^1} + \frac{2(2 - v^2)(1 + v^2)}{Y^2}$$

$$\iff G^* = \frac{Y}{4(2 - v)(1 + v)}$$
(12)

The equivalent moment of inertia I^* is defined at equation 13 with an harmonic mean of the different moments of inertia displaced at the contact point.

$$\frac{1}{I^*} = \frac{1}{I^1 + m^1 R^{1^2}} + \frac{1}{I^2 + m^2 R^{2^2}} \tag{13}$$

Normal model

The normal force is formulated as:

$$f_{ni} = k_n \Delta_{ni} + \gamma_n v_{ni} \tag{14}$$

The reaction is divided into a spring part and a damping part, with the normal stiffness k_n formulated as:

$$k_n = \frac{4}{3} Y^* \sqrt{R^* \delta} \tag{15}$$

Following the Hertz contact theory, this parameter depends mainly on the norm of the normal overlap vector δ . Thus, the normal force is not linear with respect to the overlap. The normal stiffness depends also on the equivalent Young modulus Y^* and the equivalent radius R^* defined before. The normal damping γ_n is null in this paper because the restitution coefficient e is taken at the value 1. This choice is justified in section 3.

Tangential model

The tangential force is formulated to verify the Coulomb friction law defined on the friction coefficient between particle μ_n and the normal force f_{ni} :

$$f_{ti} = -k_t \Delta_{ti} - \gamma_t v_{ti} \tag{16}$$

$$\overline{f_{ti}} \le \mu_p \overline{f_{ni}} \tag{17}$$

The reaction is divided into a spring part and a damping part. The tangential stiffness k_t is formulated as:

$$k_t = 8G^* \sqrt{R^* \delta} \tag{18}$$

Following the Hertz contact theory, this parameter depends mainly on the norm of the normal overlap vector δ . Thus, the tangential force is not linear with respect to the overlap. The tangential stiffness depends also on the equivalent shear modulus G^* and the equivalent radius R^* defined before. The tangential damping γ_t is also null in this paper because the



restitution coefficient e is taken at the value 1. This choice is justified in section 3.

Angular model

Many different angular models could be applied but an elastic–plastic spring-dashpot model is used because it is the most stable and accurate choice for simple benchmark tests [42]. Indeed, the model allows energy dissipation during relative rotation and provides packing support for static system, two main functions to verify in a particulate system [42]. The reaction moment M_i is formulated as:

$$M_i = M_i^k + M_i^d \tag{19}$$

This reaction is divided into a spring part M_i^k and a damping part M_i^d defined at equations 20 and 24:

$$M_{i,t+\Delta t}^k = M_{i,t}^k - k_r \Delta \theta_i \tag{20}$$

$$\overline{M_i^k} \le M^m \tag{21}$$

The incremental angle $\Delta\theta_i$ is obtained by a time integration of the angular velocity $\Delta\omega_i \times dt$. The angular stiffness k_r is formulated at equation 22 by considering a continuously distributed system of normal and tangential spring at the interface [42, 65].

$$k_r = 2.25k_n \mu_r^2 R^{*2} \tag{22}$$

The rolling friction coefficient μ_r is introduced. This variable is a dimensionless parameter defined as [42]:

$$\mu_r = \tan(\beta) \tag{23}$$

The angle β represents the maximum angle of a slope on which the rolling resistance moment counterbalances the moment due to gravity on the grain, see Fig. 2. The influence of μ_r is investigated in this paper.

$$M_{i,t+\Delta t}^d = \begin{cases} -C_r \Delta \omega_i & \text{if } \overline{M_{i,t+\Delta t}^k} < M^m \\ 0 & \text{if } M_{i,t+\Delta t}^k = M^m \end{cases}$$
 (24)

The damping part M_i^d is defined with a rolling viscous damping parameter C_r formulated at equation 25.

$$C_r = 2\eta_r \sqrt{I_r k_r} \tag{25}$$

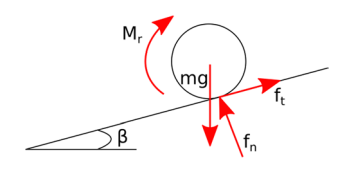
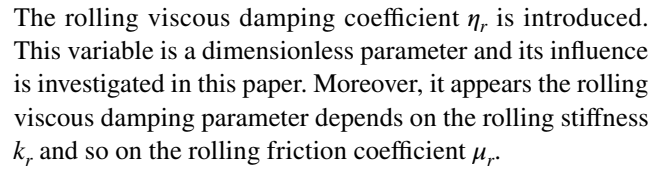


Fig. 2 Definition of the rolling resistance coefficient $\mu_r = tan(\beta)$



As described by equations 20 and 24, the spring and damping parts are restricted by a plastic behavior, the rolling of particles. The rolling starts when the spring part reaches the plastic limit M^m defined at equation 26.

$$M^m = \mu_r R^* \overline{f_{ni}} \tag{26}$$

This limit depends on the equivalent radius, the rolling friction coefficient and the normal force. Once rolling occurs, the reaction from the angular spring takes the value of M^m and the damping element is deleted.

3 Numerical model

The simulation setup is illustrated at Fig. 3. The box is a $0.004 \,\mathrm{m} \times 0.006 \,\mathrm{m} \times 0.0024 \,\mathrm{m}$ region. Faces x and z are under periodic conditions. The size of the domain has been chosen from the mean particle diameter d_{50} to respect a sufficient number of grains in all directions. On the x-axis, the shearing direction, there are $l_x/d_{50} = 4/0.26 = 15$ particles. On the z-axis, the minor direction, there are $l_z/d_{50} = 2.4/0.26 = 10$ particles. On the y-axis, the size allows the particles generation shown at Fig. 5. Sizes have been minimized to reduce the number of grains and so the computational cost, one of the main issue with DEM simulations. The gravity is not considered because its effect remains negligible under the vertical pressure applied.

The simulations, performed with the open-source software LIGGGHTS [67], consist of several steps illustrated at Fig. 5:

1. The box, bottom and top triangle plates are created. The triangle pattern represents the roughness of the plates with a geometry similar to experimental tests [68, 69].

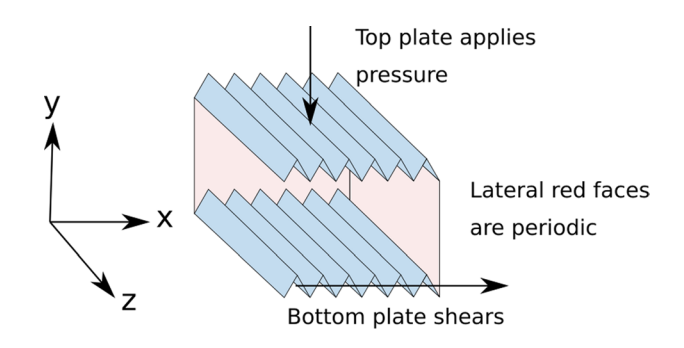
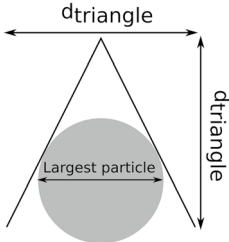


Fig. 3 The simulation box with triangle plates and periodic faces



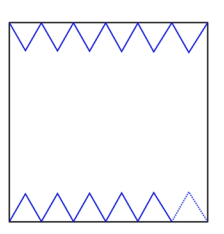
Fig. 4 Definition of the specific size of the triangle used for plates

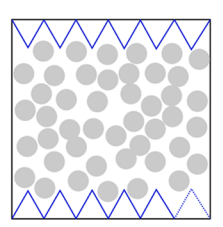


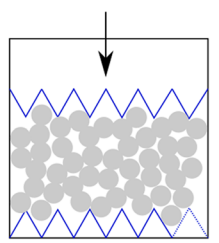
Top plate applies vertical stress of 10 MPa by moving following the y axis. This plate is free to move vertically to verify this confining and allow volume change. The value of the vertical stress has been chosen from previous experiments and numerical simulations [32, 71, 72].

The sample is sheared by moving the bottom plate at the speed of 100 μ m/s until 100% strain. This step is then repeated at the speed of 300 and 1000 μ m/s. Those

Fig. 5 The simulation is in multiple steps: creation of the box and particles, application of the normal force and shearing







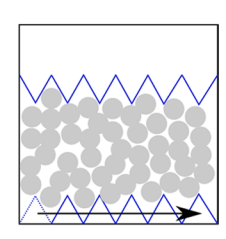


Table 1 Distribution used described by discrete radius, percentage of the mass and total number of grains

Radius	Percentage (%)	Number of parti- cles
R1 = 0.2 mm	14	2500
R2 = 0.15 mm	29	
R3 = 0.1 mm	57	

velocities have been chosen from previous numerical simulations [32] and in-situ estimations [73] to minimize the computational cost but still relevant for sheared layers in the case of landslides or fault zones.

Then, the influence of the vertical pressure is investigated. The same set-up is used except the vertical pressure (P=1)MPa and =100 MPa). The rolling friction coefficient is con-

Table 2 DEM parameters used during simulations

Variable	Short Name	Value
Simulation variables		
Time step	dt	$1,5e^{-6}$ s
Height of the sample	h	0, 005 m
Shear rate	γ'	2 - 6 - 20%
Contact stiffness number	K	400
Inertial number	I	$10^{-6} - 10^{-5}$
Mechanical variables		
Density	ρ	$2000000 kg/m^3$
Youngs modulus	Y	70 <i>GPa</i>
Poissons ratio	ν	0, 3
Restitution coefficient	e	1
Rolling friction coefficient	μ_r	0 - 0, 25 - 0, 5 - 0, 75 - 1
Rolling viscous damping coefficient	η_r	0-0,25-0,5-0,75
Friction coefficient	μ_p	0, 5

The specific size of the triangle is defined to be 1.5 times the largest particle diameter as illustrated at Fig. 4.

2. 2500 particles are generated following the distribution presented in Table 1 equivalent to the one used in [23]. This number of particles allows to get 17 particles on the height where the size of the shear band is assumed to be between $9 \times d_{50}$ and $16 \times d_{50}$ [70].

stant $\mu_r = 0,5$ and the rolling viscous damping coefficient changes $\eta_r = 0, 25, 0, 5 \text{ or } 0, 75.$

The different parameters needed for the DEM simulation are presented in Table 2 and the values have been chosen from previous articles to represent rock materials [21, 32, 47, 74]. It is important to note that the restitution coefficient



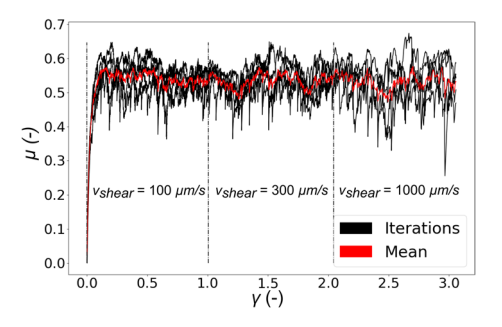


Fig. 6 Example of μ - γ curves at different shear velocities. Black lines represent the different simulations with the same $(\mu_r - \eta_r)$ configuration and the red one represents the mean curve associated to this configuration

e is equal to 1. It means there is no damping in the normal and tangential interactions. In most DEM simulations this parameter is less than 1 to introduce some energy dissipation. Indeed, in real contacts between particles damage to surface asperities and plastic yielding occur [75] but these phenomena cannot be reproduced with rigid DEM formulation. To be more realistic for the conditions considered in the present study, this coefficient should be less than 1. Nevertheless, the focus of this article is on the effect of rolling resistance and rolling damping at several shear speeds. With a restitution coefficient not equal to 1, the rate dependency in the mechanical behavior would result from the angular damping and from the restitution coefficient. Because of that, and to isolate the effect of the rolling damping, it has been chosen here to set e = 1. Moreover, Da Cruz et al. has shown there is a negligible influence of this restitution coefficient e on the mechanical behavior of a sheared sample for a dense granular flow [13].

The time step dt must verify the Rayleigh condition [66, 76] defined as:

$$dt < dt_R = \pi \times r \times \frac{\sqrt{\rho/G}}{0.1631 \times \nu + 0.8766}$$
 (27)

The time step dt must be selected considering the number of particles, the computing power, the stability of the simulation and the time scale of the test. In our case, we are looking for a 10^2 seconds term. If we include the default value $(\rho = 2500 \, \text{kg/m}^3)$ into equation 27 the time step is around 10^{-8} second and the running time skyrockets. To address this issue, we can easily change the density ρ and the shear modulus G. Those parameters are included in two dimensionless numbers defined at the equation 28: the contact stiffness number κ [13, 77] and the inertial number I [13, 33].

$$\kappa = \left(\frac{\gamma}{P(1-\nu^2)}\right)^{2/3}$$
 The contact stiffness number
$$I = \gamma' d_{50} \sqrt{\rho/P}$$
 The inertial number (28)

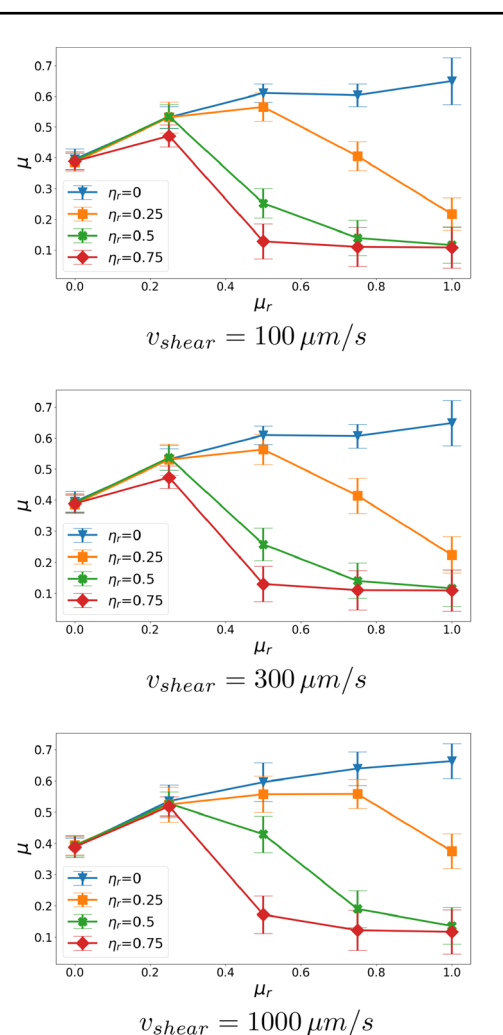


Fig. 7 Evolution of the macro friction coefficient with the rolling friction coefficient μ_r and the rolling viscous damping coefficient η_r at different shear speeds with P = 10MPa

Where $\gamma' = v_{shear}/h$ is the shear rate, h is the height of the sample during the shear, P is the pressure applied.

When these two dimensionless numbers are calculated with the values in Table 2, it appears that κ ($\kappa \leq 10^4$) lies in a range of values where the macroscopic behavior is sensitive its value as grains are not rigid enough [77]. Because of that, it is not possible to change the Young modulus Y (and so the shear modulus G). The inertial number I represents the behavior of the grains flow, which can be associated with solids, liquids or gases types of behavior [78]. This dimensionless parameter does not affect the constitutive law if the flow regime is at critical state ($I \leq 10^{-3}$) [13, 33] at the highest shear speed. In conclusion, the density ρ can be modified, if we stay under the condition $I \leq 10^{-3}$, to increase the time step and solve our computing problem. So, the density of the particles is artificially increased ($\rho = 2000000 \, kg/m^3$)



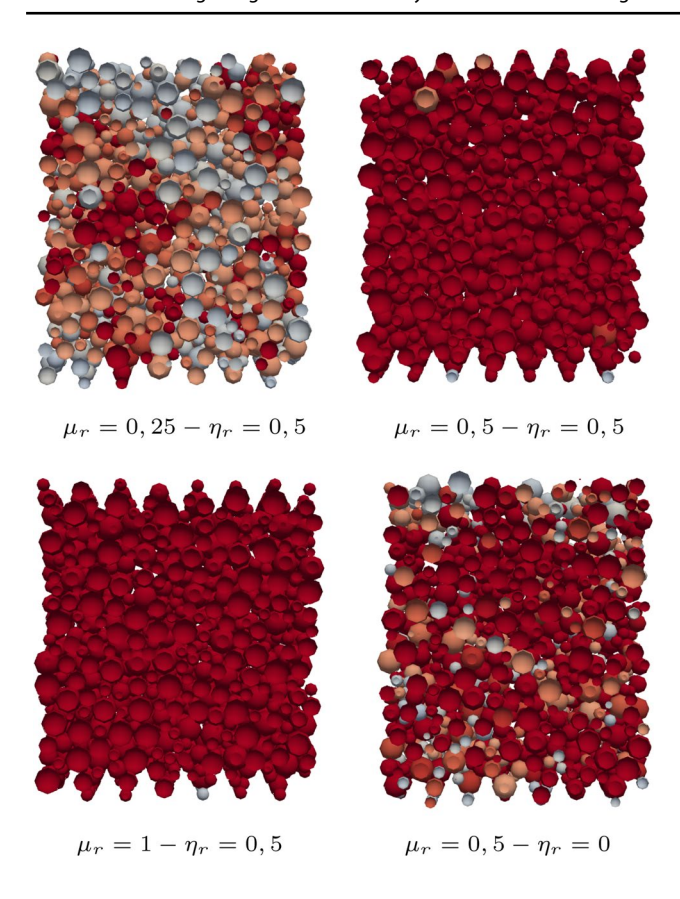


Fig. 8 Slide of sample highlighting grain rotation (rolling is in red) for several cases

during the generation step and stays constant during the entire simulation.

4 Results and discussion

Rolling Parameters Influence

A parametric study has been conducted on the influence of the rolling friction coefficient μ_r and the rolling viscous damping coefficient η_r . As Fig. 6 shows, the macro friction coefficient is plotted as a function the shear strain applied. This coefficient μ is computed by considering $\mu = F_x/F_y$, where F_x (resp. F_y) is the component following the x-axis (resp. y-axis) of the force applied on the top plate. Because of the granular aspect, there is a lot of oscillation. To reduce this noise, at least 3 simulations are run by a set of parameters (μ_r, η_r) with a different initial packing and a mean curve is computed. Moreover, only the steady-state is considered and an average value is estimated.

The comparison of the macro friction coefficient with different parameters set is highlighted at Fig. 7. It appears there is an increase of the sheared layer friction coefficient with the rolling resistance μ_r until a critical point

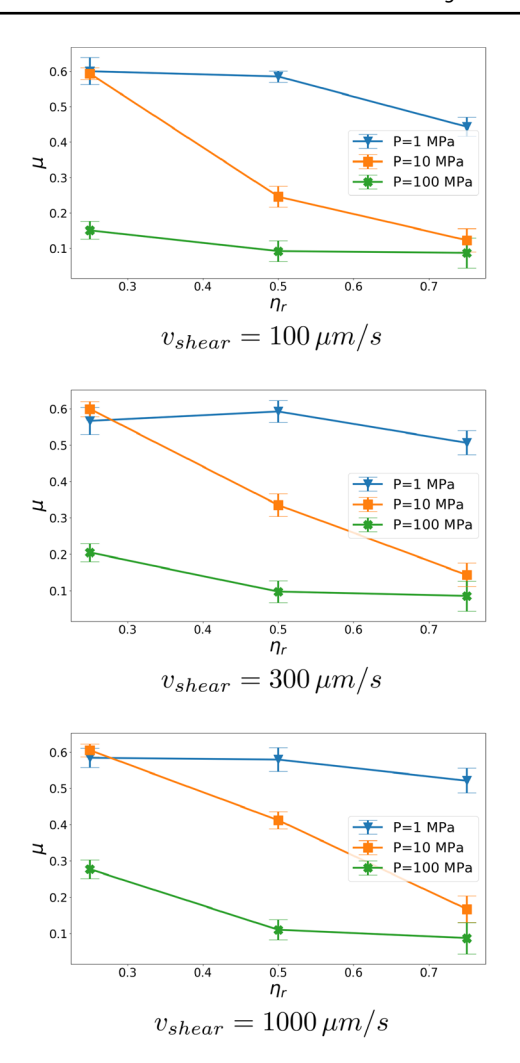


Fig. 9 Evolution of the macro friction coefficient with the rolling viscous damping coefficient η_r and the vertical pressure P at different shear speeds with $\mu_r = 0,5$

depending on the rolling damping η_r . This reduction of the macroscopic shear strength with the rolling damping is not easy to understand at first. The larger the damping is, the stiffer the system should be. Two main questions should be answered: why does the friction coefficient decrease with the rolling resistance if there is some damping? Why is the reduction larger with the damping value?

Figure 8 helps to understand this behavior. It shows the rotation of particles (in red) for four different sets of parameters. We can notice that the fewer rotations there are, the stiffer the system will be. It appears the number of rolling particles increases with the rolling resistance as can be seen on the three first plots of Fig. 8. The decrease of the friction coefficient is explained by particles rolling. Moreover, it is shown at the second and last plot of Fig. 8 that damping increases the number of rolling particles and so the friction coefficient is reduced.



36 Page 8 of 12 A. Sac-Morane et al.

Table 3 The mean	angular velocity o	on the z-axis for different	t configurations n	 P at different shear speeds

$v_{shear} = 100 \mu$ m/s					
$\eta_r =$	0.25	0.50	0.75		
1 MPa	0.3	2.2	33.7		
10 MPa	20.3	455.6	1056.2		
100 MPa	2384.5	7467.8	11774.1		
$v_{shear} = 200 \mu$ m/s					
$\overline{\eta_r} =$	0.25	0.50	0.75		
1 MPa	0.6	3.6	34.1		
10 MPa	23.9	426.6	1034.5		
100 MPa	2327.3	7564.8	11685.2		
$v_{shear} = 1000 \mu$ m/s					
$\overline{\eta_r} =$	0.25	0.50	0.75		
1 MPa	1.3	4.9	29.7		
10 MPa	28.1	342.1	1023.3		
100 MPa	2070.0	7483.6	11759.4		

A focus on the model equations must be done at relation 29 to understand better those observations (the input rolling parameters are emphasized in red). First, it appears the increment of the spring ΔM_r^k depends on μ_r^2 while the plastic limit $\mu_r R^* f_n$ depends only on μ_r . There is a square factor between those values. Thus, this plastic limit, and so grain rolling, is reached easier with a larger rolling resistance μ_r for a same angular displacement θ .

$$M^{m} = \mu_{r} R^{*} f_{n} \Delta M_{r}^{k} = -2,25 k_{n} \mu_{r}^{2} R^{*2} \Delta \theta$$

$$M_{r,t+\Delta t}^{d} = \begin{cases} \text{if } |M_{r,t+\Delta t}^{k}| < \mu_{r} R^{*} f_{n} : \\ -2 \eta_{r} \mu_{r} \sqrt{2,25 I_{r} k_{n}} \omega \end{cases}$$

$$\text{if } |M_{r,t+\Delta t}^{k}| = \mu_{r} R^{*} f_{n} :$$

$$0$$
(29)

Concerning the damping, it avoids the variation of the angular position $(\Delta\omega \to 0)$ during the elastic phase. As we have seen before, the main part of the sample is at the plastic phase and particles roll. So, the damping acts in opposition to the angular spring, keeping grain into the plastic phase. We can notice that we have decided in this paper to shut down the damping moment when the angular plastic limit is reached (see equation 29) following the model of [42].

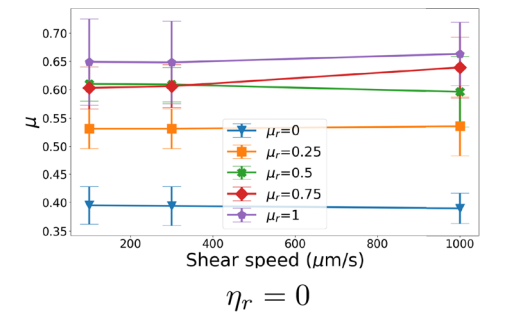
In this way, we can understand better the reduction of the friction coefficient with the rolling stiffness μ_r if damping is active. We can notice no decrease but an increase of the friction coefficient in the case of no damping. In the absence of this one, the angular spring can act normally. The larger the rolling parameter is, the stiffer the global sample is.

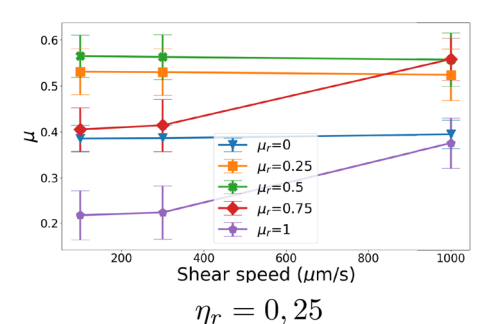
This observation can be useful to understand the mechanical behavior of granular materials subjected to damage. Experiments and simulations have highlighted that particles tend to become less or more [79–81, 84] rounded under large deformation due to damage. The work of Buscarnera and Einav, extending the Continuum Breakage Mechanics, reconciles those conflicting observations [82]. Shape descriptors are converging to attractors. The evolution of the aspect ratio α , related to the grain morphology, is plotted following a breakage parameter B and the stress σ . It is highlighted that from different initial values the aspect ratio converges to the same value, the attractor. Remember that rolling friction is a technique to model particle shape in DEM to minimize computational cost [63] and that a calibration law between the rolling friction and the degree of true sphericity of the grain has already been developed [64]. This index is an easy way to measure how a particle is similar to a sphere. Notice that the aspect ratio used by Buscarnera and Einav and the degree of the true sphericity used by Rorato et al. are not the same definition but represent the same idea. It appears with this calibration that the rolling friction decreases as the grain becomes more spherical. Softening and hardening behaviors can be understood thanks to our work, the shape evolution with the breakage and the relation between the shape and the rolling friction coefficient. In this paper, we have considered sheared samples with constant rolling friction during the simulation. But, this opens further investigations, considering rolling friction varying during simulation as a function of a damage parameter. For example, if the aspect ratio or the degree of true sphericity decreases during the test, particles become less rounded, the rolling friction coefficients increase, and the sample shear strength evolves depending on the position of the critical point (softening or hardening).

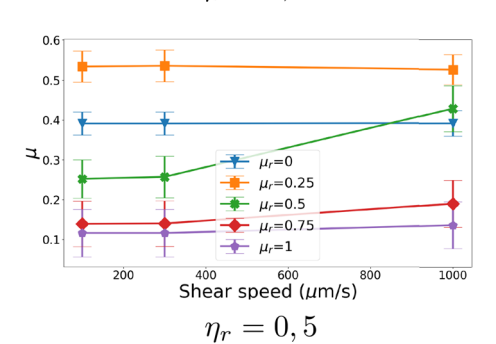
Vertical Pressure Influence











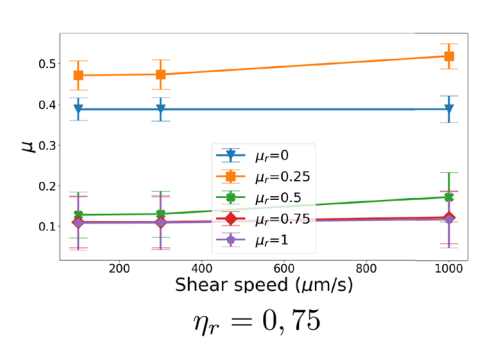


Fig. 10 Evolution of the sample friction coefficient with the shear speed and the rolling friction coefficient μ_r at different rolling viscous damping coefficients with P = 10 MPa

Equation 29 highlights the plastic moment depends on normal forces f_n (and so on vertical pressure P). Figure 9 illustrates the evolution of the macro friction coefficient with different vertical pressure P and rolling viscous damping coefficient η_r .

The critical point defined previously (point before which the friction weakening appears) depends on the vertical pressure. This behavior has already been observed [32, 83]. The importance of the rolling increases with the vertical pressure. The mean angular velocity ω_z on the z-axis have been computed over configurations $P - \eta_r - v_{shear}$ at Table 3. It is highlighted that the vertical pressure P favours the grain rolling. That is why a friction weakening occurs with this parameter.

Speed Influence

Figure 10 highlights the shearing speed influence on the system. It is the same results as before but plotted in another way. No speed effect is visible in most simulations as the friction coefficient keeps the same value. It is not surprising that no speed effects are spotted because there are no other parameters except the damping parameter which depends on speed or time. A speed influence is nevertheless noticed for cases where the friction coefficient starts to decrease with rolling resistance (for example the case $\mu_r = 0.5$ and $\eta_r = 0, 5$ at Fig. 10). As shown at Fig. 8 for this set, few particles (in orange or in white) are still not rolling during this critical step. The damping value is not large enough to cancel the effect of the spring and few grains are in the elastic phase. The damping creates so in this case a speed influence. If the damping value is larger, we have seen particles tend to be all in the plastic phase. If it is lower, the damping is negligible or null. In both cases, the speed effect disappears.

5 Conclusion

In this paper, we have considered granular materials into a plane shear configuration to investigate the effect of the rolling resistance and damping on the macroscopic friction coefficient. Thanks to numerical DEM simulations, the relation between those parameters becomes clearer. It appears:

- 1. In the no damping case, the sample stiffness increases with the rolling resistance.
- The consideration of the rolling damping introduces a critical point. For a constant damping value, the sample stiffness increases the rolling parameter until this critical point is reached. Then, the stiffness starts to decrease until a residual value. Hence, the damping tends to act against the spring and grains roll. The choice of the angular damping, used in previous papers mainly for stability reasons, should be well thought out.
- 3. No visible speed effects have been highlighted except at the critical point. For the same rolling resistance value: (i) When the damping parameter is not large enough, the angular spring is the main element and no speed dependency is spotted, (ii) when the damping parameter is too large, all grains are in the plastic phase (roll) and



the residual value is reached and (iii) when the damping parameter is at critical value, there is no main element in the rolling model, speed dependency occurs.

Acknowledgements Computational resources have been provided by the Consortium des Équipements de Calcul Intensif (CÉCI), funded by the Fonds de la Recherche Scientifique de Belgique (F.R.S.-FNRS) under Grant No. 2.5020.11 and by the Walloon Region. Support by the CMMI-2042325 project is also acknowledged.

Declarations

Conflict of interest The authors declare that they have no conflict of interest.

References

- Myers, R., Aydin, A.: The evolution of faults formed by shearing across joint zones in sandstone. J. Struct. Geol. 26, 947–966 (2004). https://doi.org/10.1016/j.jsg.2003.07.008
- Poulet, T., Veveakis, M., Herwegh, M., Buckingham, T., Regenauer-Lieb, K.: Modeling episodic fluid-release events in the ductile carbonates of the Glarus thrust. Geophys. Res. Lett. 41, 7121–7128 (2014). https://doi.org/10.1002/2014GL061715
- Segui, C., Rattez, H., Veveakis, M.: On the stability of deep-seated landslides. The cases of Vaiont (Italy) and Shuping (Three Gorges Dam, China). J. of Geophys. Res. Earth Surf 125, e2019JF005203 (2020). https://doi.org/10.1029/2019JF005203
- Iverson, R.M.: The physics of debris flows. Rev. Geophys. 35, 245–296 (1997). https://doi.org/10.1029/97RG00426
- Sulem, J., Vardoulakis, I.G.: Bifurcation Analysis in Geomechanics, 1st edn. CRC Press, London (1995). https://doi.org/10.1201/9781482269383
- Sulem, J., Stefanou, I., Veveakis, M.: Stability analysis of undrained adiabatic shearing of a rock layer with Cosserat microstructure. Granul. Matter 13, 261–268 (2011). https://doi.org/10.1007/s00603-018-1529-7
- Rattez, H., Stefanou, I., Sulem, J.: The importance of Thermo-Hydro-Mechanical couplings and microstructure to strain localization in 3D continua with application to seismic faults. Part I: theory and linear stability analysis. J. Mech. Phys. Solids 115, 54–76 (2018). https://doi.org/10.1016/j.jmps.2018.03.004
- Rattez, H., Stefanou, I., Sulem, J., Veveakis, M., Poulet, T.: The importance of Thermo-Hydro-Mechanical couplings and microstructure to strain localization in 3D continua with application to seismic faults Part II: Numerical implementation and postbifurcation analysis. J. Mech. Phys. Solids. 115, 1–29 (2018). https://doi.org/10.1016/j.jmps.2018.03.003
- Rattez, H., Stefanou, I., Sulem, J., Veveakis, M., Poulet, T.: Numerical analysis of strain localization in rocks with thermohydro-mechanical couplings using Cosserat continuum. Rock Mech. Rock Eng. 51, 3295–3311 (2018). https://doi.org/10. 1007/s00603-018-1529-7
- Papachristos, E., Stefanou, I., Sulem, J.: A discrete elements study of the frictional behavior of fault gouges. J. Geophys. Res. Solid Earth. 128, e2022JB025209 (2023). https://doi.org/ 10.1029/2022JB025209
- Dubois, F., Acary, V., Jean, M.: The Contact Dynamics method: a nonsmooth story. C. R. Méc. 346, 247–262 (2018). https://doi. org/10.1016/j.crme.2017.12.009

- Burman, B.C., Cundall, P.A., Strack, O.D.L.: A discrete numerical model for granular assemblies. Geotech. 30, 331–336 (1980). https://doi.org/10.1680/geot.1980.30.3.331
- Da Cruz, F., Emam, S., Prochnow, M., Roux, Chevoir: Rheophysics of dense granular materials: discrete simulation of plane shear flows. Rev. E Stat. Nonlinear Soft Matter Phys. 72, 1–17 (2005). https://doi.org/10.1103/PhysRevE.72.021309
- Imole, O.I., Wojtkowski, M., Magnanimo, V., Luding, S.: Micro-macro correlations and anisotropy in granular assemblies under uniaxial loading and unloading. Phys. Rev. E 89, 042210 (2014). https://doi.org/10.1103/PhysRevE.89.042210
- González, S., Windows-Yule, C.R.K., Luding, S., Parker, D.J., Thornton, A.R.: Forced axial segregation in axially inhomogeneous rotating systems. Phys. Rev. E 92, 022202 (2015). https://doi. org/10.1103/PhysRevE.92.022202
- O'Sullivan, C.: Particulate Discrete Element Modelling: A Geomechanics Perspective. CRC Press, London (2011). https:// doi.org/10.1201/9781482266498
- Hanley, K.J., O'Sullivan, C., Huang, X.: Particle-scale mechanics of sand crushing in compression and shearing using DEM. Soils and Found. 55, 1100–1112 (2015). https://doi.org/10.1016/j.sandf.2015.09.011
- Zhang, N., Ciantia, M.O., Arroyo, M., Gens, A.: A contact model for rough crushable sand. Soils and Found. 61, 798–814 (2021). https://doi.org/10.1016/j.sandf.2021.03.002
- Elliott, D., Rutter, E.: The kinetics of rock deformation by pressure solution. Philos. Trans. R. Soc. A Math. Phys. Eng. Sci 283, 218–219 (1976). https://doi.org/10.1098/rsta.1976.0079
- Florian, K.L.: A model for intergranular pressure solution in open systems. Tectonophys. 245, 153–170 (1995). https://doi. org/10.1016/0040-1951(94)00232-X
- van den Ende, M..P..A., Marketos, G., Niemeijer, A..R., Spiers, C..J.: Investigating compaction by intergranular pressure solution using the discrete element method. J. Geophys. Res. Solid Earth 123, 107–124 (2018). https://doi.org/10.1002/2017J B014440
- Abe, S., Dieterich, J.H., Mora, P., Place, D.: Simulation of the influence of rate- and state-dependent friction on the macroscopic behavior of complex fault zones with the lattice solid model. Pure Appl. Geophys. 159, 1967–1983 (2002). https://doi.org/10.1007/ s00024-002-8718-7
- Morgan, J.K.: Particle dynamics simulations of rate- and state-dependent frictional sliding of granular fault gouge. Pure Appl. Geophys. 161, 1877–1891 (2004). https://doi.org/10.1007/s00024-004-2537-y
- Potyondy, D..O., Cundall, P..A.: A bonded-particle model for rock. Int. J. Rock Mech. Min. Sci. 41, 1329–1364 (2004). https://doi. org/10.1016/j.ijrmms.2004.09.011
- Zhao, H., Sang, Y., Deng, A., Ge, L.: Influences of Stiffness Ratio, Friction Coefficient and Strength Ratio on the Macro Behavior of Cemented Sand Based on DEM. In: Li, X., Feng, Y., Mustoe, G. (eds) DEM 2016: Proceedings of the 7th International Conference on Discrete Element Methods, pp. 485-495. Springer, Singapore (2017). https://doi.org/10.1007/978-981-10-1926-5_51
- Casas, N., Mollon, G., Daouadji, A.: Cohesion and Initial porosity
 of granular fault gouges control the breakdown energy and the
 friction law at the onset of sliding. ESS Open Archive (2020).
 https://doi.org/10.1002/essoar.10504966.1
- Soulié, F., El Youssoufi, M.S., Cherblanc, F., Saix, C.: Capillary cohesion and mechanical strength of polydisperse granular materials. Eur. Phys. J. E 21, 349–357 (2006). https://doi.org/10.1140/epje/i2006-10076-2
- Vardoulakis, I.: Dynamic thermo-poro-mechanical analysis of catastrophic landslides. Géotech 52, 157–171 (2002). https://doi. org/10.1680/geot.2002.52.3.157



- Rice, J..R.: Heating and weakening of faults during earthquake slip. J. Geophys. Res. Solid Earth 111, B05311 (2006). https:// doi.org/10.1029/2005JB004006
- Gan, Y., Rognon, P., Einav, I.: Phase transitions and cyclic pseudotachylyte formation in simulated faults. Philos. Mag. 92, 3405
 – 3417 (2012). https://doi.org/10.1080/14786435.2012.669062
- 31. Mollon, G., Aubry, J., Schubnel, A.: Simulating melting in 2D seismic fault gouge. J. Geophys. Res. Solid Earth **126**, 6 (2021). https://doi.org/10.1029/2020JB021485
- Ferdowsi, B., Rubin, A..M.: A granular physics-based view of fault friction experiments. J. Geophys. Res. Solid Earth 125, 1–32 (2020). https://doi.org/10.1029/2019JB019016
- 33. Midi, G.D.R.: On dense granular flows. Eur. Phys. J. E **14**, 341–365 (2004). https://doi.org/10.1140/epje/i2003-10153-0
- Estrada, N., Taboada, A., Radjaï, F.: Shear strength and force transmission in granular media with rolling resistance. Phys. Rev. E Stat. Nonlinear Soft Matter Phys 78, 1–11 (2008). https://doi.org/10.1103/PhysRevE.78.021301
- Binaree, T., Azéma, E., Estrada, N., Renouf, M., Preechawuttipong, I.: Combined effects of contact friction and particle shape on strength properties and microstructure of sheared granular media. Phys. Rev. E 102, 22901 (2020). https://doi.org/10.1103/PhysRevE.102.022901
- Oda, M., Takemura, T., Takahashi, M.: Microstructure in shear band observed by microfocus X-ray computed tomography. Géotech 54, 539–542 (2004). https://doi.org/10.1680/geot.2004.54.8.
- Oda, M., Konishi, J., Nemat-Nasser, S.: Experimental micromechanical evaluation of strength of granular materials: Effects of particle rolling. Mech. of Mater. 1, 269–283 (1982). https://doi. org/10.1016/0167-6636(82)90027-8
- Zhou, Y..C., Wright, B..D., Yang, R..Y., Xu, B..H., Yu, A..B.: Rolling friction in the dynamic simulation of sandpile formation. Phys. A Stat. Mech. Appl 269, 536–553 (1999). https://doi.org/ 10.1016/S0378-4371(99)00183-1
- Alonso-Marroquin, F., Vardoulakis, I., Herrmann, H.J., Weatherley, D., Mora, P.: Effect of rolling on dissipation in fault gouges. Phys. Rev. E - Stat. Nonlinear Soft Matter Phys 74, 1–10 (2006). https://doi.org/10.1103/PhysRevE.74.031306
- Papanicolopulos, S.A., Veveakis, E.: Sliding and rolling dissipation in Cosserat plasticity. Granul. Matter 13, 197–204 (2011). https://doi.org/10.1007/s10035-011-0253-8
- 41. Zhao, C., Li, C.: Influence of rolling resistance on the shear curve of granular particles. Phys. A Stat. Mech. and Appl **460**, 44–53 (2016). https://doi.org/10.1016/j.physa.2016.04.043
- Ai, J., Chen, J.F., Rotter, J.M., Ooi, J.Y.: Assessment of rolling resistance models in discrete element simulations. Powder Technol. 206, 269–282 (2011). https://doi.org/10.1016/j.powtec.2010. 09.030
- 43. Iwashita, K., Oda, M.: Rolling Resistance At Contacts in Simulation of Shear Band. Asce **124**, 285–292 (1998). https://doi.org/10. 1061/(ASCE)0733-9399(1998)124:3(285)
- Iwashita, K., Oda, M.: Micro-deformation mechanism of shear banding process based on modified distinct element method. Powder Technol. 109, 192–205 (2000). https://doi.org/10.1016/ S0032-5910(99)00236-3
- Murakami, A., Sakaguchi, H., Hasegawa, T.: Dislocation, vortex and couple stress in the formation of shear bands under trap-door problems. Soils and found. 37, 123–135 (1997). https://doi.org/ 10.3208/sandf.37.123
- Zhang, W., Wang, J., Jiang, M.: DEM-aided discovery of the relationship between energy dissipation and shear band formation considering the effects of particle rolling resistance. J. Geotech. Geoenviron. Eng. 139, 1512–1527 (2013). https://doi.org/10.1061/(asce)gt.1943-5606.0000890

- 47. Tang, H., Dong, Y., Chu, X., Zhang, X.: The influence of particle rolling and imperfections on the formation of shear bands in granular material. Granul. Matter **18**, 1–12 (2016). https://doi.org/10.1007/s10035-016-0607-3
- Nho, H., Nguyen, G., Scholtès, L., Guglielmi, Y., Victor, F.: Micromechanics of sheared granular layers activated by fluid pressurization Micromechanics of sheared granular layers activated by fluid pressurization. Geophys. Res. Lett. 48, e2021GL093222 (2021). https://doi.org/10.1002/essoar.10506504.1
- Yang, Y., Cheng, Y.M., Sun, Q.C.: The effects of rolling resistance and non-convex particle on the mechanics of the undrained granular assembles in 2D. Powder Technol. 318, 528–542 (2017). https://doi.org/10.1016/j.powtec.2017.06.027
- Liu, Y., Liu, H., Mao, H.: The influence of rolling resistance on the stress-dilatancy and fabric anisotropy of granular materials. Granul. Matter 20, 12 (2018). https://doi.org/10.1007/ s10035-017-0780-z
- Barnett, N., Mizanur Rahman, M.D., Rajibul Karim, M.D., Nguyen, H.B.K.: Evaluating the particle rolling effect on the characteristic features of granular material under the critical state soil mechanics framework. Granul. Matter 22, 89 (2020). https:// doi.org/10.1007/s10035-020-01055-5
- Godet, M.: The third-body approach: a mechanical view of wear. Wear 100, 437–452 (1984). https://doi.org/10.1016/0043-1648(84)90025-5
- Colas, G., Saulot, A., Godeau, C., Michel, Y., Berthier, Y.: Decrypting third body flows to solve dry lubrication issue - MoS2 case study under ultrahigh vacuum. Wear 305, 192–204 (2013). https://doi.org/10.1016/j.wear.2013.06.007
- 54. Jensen, R.P., Bosscher, P.J., Plesha, M.E., Edil, T.B.: DEM simulation of granular media-structure interface: effects of surface roughness and particle shape. Int J Numer Anal Methods Geomech. 23, 531–547 (1999)
- Kozicki, J., Tejchman, J.: Numerical simulations of sand behavior using DEM with two different descriptions of grain roughness. In: Oñate, E., Owen, D.R.J. (Eds) II International Conference on Particle-based Methods - Fundamentals and Applications. Particles 2011 (2011)
- Mollon, G., Quacquarelli, A., Andò, E., Viggiani, G.: Can friction replace roughness in the numerical simulation of granular materials? Granul. Matter 22, 42 (2020). https://doi.org/10.1007/s10035-020-1004-5
- Garcia, X., Latham, J.P., Xiang, J., Harrison, J.: A clustered overlapping sphere algorithm to represent real particles in discrete element modelling. Geotech. 59, 779–784 (2009). https://doi.org/ 10.1680/geot.8.T.037
- Podlozhnyuk, A.: Modelling superquadric particles in DEM and CFD-DEM: implementation, validation and application in an open-source framework. (2018)
- Cundall, P.: Formulation of a three-dimensional distinct element model-Part I. A scheme to detect and represent contacts in a system composed of many polyhedral blocks. Int. J. Rock Mech. Min. Sci. Geomech 25, 107–116 (1988). https://doi.org/10.1016/ 0148-9062(88)92293-0
- Nezami, E.G., Hashash, Y.M.A., Zhao, D., Ghaboussi, J.: A fast contact detection algorithm for 3-D discrete element method. Comput. Geotech. 31, 575–587 (2004). https://doi.org/10.1016/j. compgeo.2004.08.002
- Alonso-Marroquin, F., Wang, Y.: An efficient algorithm for granular dynamics simulations with complex-shaped objects. Granul. Matter 11, 317–329 (2009). https://doi.org/10.1007/ s10035-009-0139-1
- Estrada, N., Azéma, E., Radjai, F., Taboada, A.: Identification of rolling resistance as a shape parameter in sheared granular media. Phys. Rev. E - Stat. Nonlinear Soft Matter. Phys. 84, 1–2 (2011). https://doi.org/10.1103/PhysRevE.84.011306



36 Page 12 of 12 A. Sac-Morane et al.

 Wensrich, C.M., Katterfeld, A.: Rolling friction as a technique for modelling particle shape in DEM. Powder Technol. 217, 409–417 (2012). https://doi.org/10.1016/j.powtec.2011.10.057

- Rorato, R., Arroyo, M., Gens, A., Andò, E., Viggiani, G.: Image-based calibration of rolling resistance in discrete element models of sand. Comput. Geotech. 131, 103929 (2021). https://doi.org/10.1016/j.compgeo.2020.103929
- Jiang, M.J., Yu, H.S., Harris, D.: A novel discrete model for granular material incorporating rolling resistance. Comput. Geotech.
 32, 340–357 (2005). https://doi.org/10.1016/j.compgeo.2005.05.
- Johnson, K.L.: Contact Mechanics. Cambridge University Press, London (1985). https://doi.org/10.1017/CBO9781139171731
- Kloss, C., Goniva, C., Hager, A., Amberger, S., Pirker, S.: Models, algorithms and validation for opensource DEM and CFD-DEM. Prog. Comput. Fluid Dyn. 12, 140–152 (2012). https://doi.org/10. 1504/PCFD.2012.047457
- Anthony, J., Marone, C.: Influence of particle characteristics on granular friction. J. Geophys. Res. Solid Earth 110, 1–14 (2005). https://doi.org/10.1029/2004JB003399
- Koval, G., Chevoir, F., Roux, J.N., Sulem, J., Corfdir, A.: Interface roughness effect on slow cyclic annular shear of granular materials. Granul. Matter 13, 525–540 (2011). https://doi.org/10.1007/ s10035-011-0267-2
- Rattez, H., Shi, Y., Sac-Morane, A., Klaeyle, T., Mielniczuk, B., Veveakis, M.: Effect of grain size distribution on the shear band thickness evolution in sand. Géotech. 72, 350–363 (2020). https:// doi.org/10.1680/jgeot.20.P.120
- Dieterich, J..H.: Modeling of rock friction 1. Experimental results and constitutive equations. J. Geophys. Res. Solid Earth 84, 2161– 2168 (1979). https://doi.org/10.1029/JB084iB05p02161
- Morrow, C.A., Byerlee, J.D.: Experimental studies of compaction and dilatancy during frictional sliding on faults containing gouge. J. Struct. Geol. 11, 815–825 (1989). https://doi.org/10.1016/0191-8141(89)90100-4
- Beroza, G.C., Jordan, T.H.: Searching for slow and silent earth-quakes using free oscillations. J. Geophys. Res. 95, 2485–2510 (1990). https://doi.org/10.1029/JB095iB03p02485
- Idrissi, H., Samaee, V., Lumbeeck, G., van der Werf, T., Pardoen, T., Schryvers, D., Cordier, P.: In situ quantitative tensile testing of antigorite in a transmission electron microscope. J. Geophys. Res Solid Earth 125, 1–12 (2020). https://doi.org/10.1029/2019J B018383
- Cavarretta, I., Coop, M., O'Sullican, C.: The influence of particle characteristics on the behaviour of coarse grained soils. Geotech.
 413–424 (2010). https://doi.org/10.1680/geot.2010.60.6.413

- Thornton, C., Randall, C.W.: Applications of theoretical contact mechanics to solid particle system simulation. Micromech. Granul. Mater. 20, 133–142 (1988). https://doi.org/10.1016/B978-0-444-70523-5.50023-0
- Roux, J.N., Combe, G.: Quasistatic rheology and the origins of strain. C. R. Phys. 3, 131–140 (2002). https://doi.org/10.1016/ \$1631-0705(02)01306-3
- Jaeger, H.M., Nagel, S.R., Behringer, R.P.: Granular solids, liquids, and gases. Rev. Mod. Phys. 68, 1259–1273 (1996). https://doi.org/10.1103/RevModPhys.68.1259
- Zhu, F., Zhao, J.: Interplays between particle shape and particle breakage in confined continuous crushing of granular media. Powder Technol. 378, 455–467 (2021). https://doi.org/10.1016/j.powtec.2020.10.020
- Ueda, T., Matsushima, T., Yamada, Y.: DEM simulation on the one-dimensional compression behavior of various shaped crushable granular materials. Granul. Matter 15, 675–684 (2013). https:// doi.org/10.1007/s10035-013-0415-y
- Zhang, X., Hu, W., Scaringin, G., Baudet, B.A., Han, W.: Particle shape factors and fractal dimension after large shear strains in carbonate sand. Geotech. Lett. 8, 73–79 (2018). https://doi.org/ 10.1680/jgele.17.00150
- Buscarnera, G., Einav, I.: The mechanics of brittle granular materials with coevolving grain size and shape. Proc. R. Soc. A 477, 20201005 (2021). https://doi.org/10.1098/rspa.2020.1005
- Morgan, J..K.: Numerical simulations of granular shear zones using the distinct element method. 2. Effects of particle size distribution and interparticle friction on mechanical behavior. J. of Geophys. Res.: Solid Earth 104, 2721–2732 (1999). https://doi. org/10.1029/1998jb900055
- Rattez, H., Disidoro, F., Sulem, J., Veveakis, M.: Influence of dissolution on long-term frictional properties of carbonate fault gouge. Geomech. Energy Environ. 26, 100234 (2021). https://doi. org/10.1016/j.gete.2021.100234

Publisher's Note Springer Nature remains neutral with regard to jurisdictional claims in published maps and institutional affiliations.

Springer Nature or its licensor (e.g. a society or other partner) holds exclusive rights to this article under a publishing agreement with the author(s) or other rightsholder(s); author self-archiving of the accepted manuscript version of this article is solely governed by the terms of such publishing agreement and applicable law.

